Pilot signal design via constrained optimization with application to delay-Doppler shift estimation in OFDM systems

Jing, Lishuai; Pedersen, Troels; Fleury, Bernard Henri

Published in:
51st Annual Allerton Conference on Communication, Control, and Computing

DOI (link to publication from Publisher):
10.1109/Allerton.2013.6736519

Publication date:
2013

Document Version
Publisher's PDF, also known as Version of record

Pilot Signal Design via Constrained Optimization with Application to Delay-Doppler Shift Estimation in OFDM Systems

Lishuai Jing[1], Troels Pedersen[1] and Bernard H. Fleury[1]

***Abstract*— We address the problem of searching for the optimal pilot signal, i.e. pattern and signature, of an orthogonal frequency-division multiplexing (OFDM) system when the purpose is to estimate the delay and Doppler shift under the assumption of a single-path propagation channel. This problem is relevant for synchronization and for time-based localization using said signals. We propose to use the Cramér-Rao bound and the normalized side-lobe level (NSL) of the ambiguity function as figures of merit to devise the pilot signals. We formulate the design problem as a constrained optimization problem for which we propose a genetic algorithm that computes close-to-optimal solutions. Simulation results demonstrate that the proposed algorithm can efficiently find pilot signals that outperform the state-of-the-art pilot signals in both single-path and multipath propagation scenarios. In addition, we demonstrate that data interference causes a performance loss if a standard non-coherent correlator is used. The results also indicate that the pilot pattern impacts the estimator's performance more than the pilot signature.**

I. INTRODUCTION

In Orthogonal Frequency-Division Multiplexing (OFDM) systems, data signals are embedded in an OFDM frame together with pilot signals which are used to acquire channel information [1]. In this contribution, the term pilot signal embraces the pilot pattern (i.e. the placement of pilots in the time-frequency grid) and the pilot signature (i.e. pilot amplitudes and phases). The traditional objective of pilot signal design is to find parsimonious pilot signals that lead to efficient channel estimation in OFDM receivers. A comprehensive survey of pilot signal design can be found in [1]. Equispaced and equipowered pilot signals are shown to maximize the channel capacity, minimize the channel estimation error, and minimize the bit error rate for the considered scenarios, see [1] and references therein.

The last ten years have witnessed a steady increasing endeavor in research on localization using terrestrial wireless systems, especially long-term evolution (LTE) and its extension LTE-A. The deployment of localization capabilities in terrestrial wireless systems is aimed at substituting, complementing, or supplementing satellite-based positioning systems in scenarios where the latter systems are unable to operate [2] [3] [4]. These localization features put additional requirements on the pilot signals transmitted by these wireless systems: pilot signals should additionally be designed to optimze positioning capabilities. Position-bearing channel parameters commonly exploited for localization are the received signal strength (RSS), the propagation delay, and the angle of arrival (AOA) [2] [4]. Time-of-arrival (TOA) and time-difference-of-arrival (TDOA) based positioning methods rely on estimates of the propagation delay between the reference stations and the mobile station to be localized. Doppler shift estimate can be used to extract the relative velocity for navigation and thereby to enhance the positioning accuracy [3]. In this contribution, we focus on pilot assisted delay and Doppler shift estimation in OFDM for the purpose of synchronization and localization.

In radar theory, the ambiguity function [5] of the transmit signal is an important tool for assessing the accuracy of the joint estimation of the delay and Doppler shift. To achieve good estimation accuracy, it is mandatory that the ambiguity function exhibits a narrow main-lobe and low side-lobes. However, these two features are contradictory due to the volume invariance property [5]. The ambiguity function of equispaced and equipowered pilot signals does not fulfill the second of these requirements: it exhibits high side-lobes (see Fig. 2 in Section V). Two approaches have been proposed in the literature to obtain pilot signals with a "good" ambiguity function in the aforementioned sense. The first approach consists in using pilot patterns that belong to the class of "perfect periodic" Costas arrays [6]. This class is an extension of the class of Costas arrays. Costas arrays leads to an ambiguity function with low side-lobes away from the main-lobe, though high side-lobes remain near the main-lobe [7]. A limitation of the Costas arrays is their inherent constraint: the array must be square and the number of pilots must equal the array length. The class of "perfect periodic" Costas arrays [6] allow for alleviating this constraint. The second approach, proposed in [8], is to use a genetic algorithm to design pilot signals for one OFDM symbol that yields an autocorrelation function—the delay ambiguity function in our terminology—with low side-lobes. The objective function that the algorithm attempts to minimize is a linear combination of the maximum side-lobe magnitude and the 3 dB main-lobe width of the delay ambiguity function.

Inspired by the above two approaches, we consider in this contribution the constrained optimization problem of designing pilot signals that yield a delay-Doppler ambiguity function with low side-lobes, while keeping the Cramér-Rao bounds (CRBs) for the estimation of the delay and Doppler shift below a prescribed level. We propose a genetic algorithm to compute close-to-optimal solutions. For a given number of pilots, the algorithm can efficiently find pilot signals which yield lower side-lobes and CRBs than the

[1]Lishuai Jing, Troels Pedersen, and Bernard H. Fleury are with the Section Navigation and Communications (NavCom), Dept. of Electronic Systems, Aalborg University, Denmark {lji, troels, fleury}@es.aau.dk

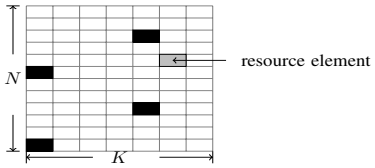

Fig. 1. The structure of an OFDM frame with $N = 12$ subcarriers and $K = 7$ OFDM symbols. One box stands for one resource element. Black boxes indicate pilot symbols and white boxes indicate data symbols.

corresponding values achieved with equispaced, equipowered pilot signals and "perfect periodic" Costas arrays. We provide simulation results showing that the pilot signals designed with the genetic algorithm lead to a better estimation accuracy compared to the accuracy achieved by using "perfect periodic" Costas arrays in both single-path and multipath channels when the delay-Doppler estimator is implemented via a standard (pilot-based) correlator. The results also show that the pilot pattern affects the estimator performance more than the pilot signature and that the data symbols affect the threshold region performance of the correlator-based delay-Doppler estimator.

II. SIGNAL MODEL

We consider a single-input single-output OFDM setup with N subcarriers and K symbols in a frame as the example shown in Fig. 1. An OFDM symbol with time duration T is generated by multiplexing a sequence of data symbols and known pilot symbols onto N orthogonal sub-carriers. Afterward, the time domain symbols are obtained by using an inverse Fourier transform. Finally, a cyclic prefix of duration $T_{\rm cp}$ is appended to prevent inter-symbol and inter-carrier interference. The total duration of an OFDM symbol is thus $T_{\rm p} = T + T_{\rm cp}$. The adjacent sub-carrier spacing is $\Delta f = \frac{1}{T}$.

An OFDM frame consists of a total of NK so-called resource elements indexed by the set $\mathbf{I} = \{1, 2, \ldots, NK\}$. Of these resource elements, $N_{\rm p} = |\mathbf{I}_{\rm p}|$ are pilots indexed by $\mathbf{I}_{\rm p}$ and $N_{\rm d} = |\mathbf{I}_{\rm d}|$ are allocated to data indexed by $\mathbf{I}_{\rm d}$. We further define the mapping

$$\mathbf{I} \to \{1, \ldots, N\} \times \{1, \ldots, K\} : i \mapsto (n(i), k(i)), \qquad (1)$$

where $n(i)$ and $k(i)$ specify the subcarrier and the OFDM symbol respectively of resource element i. The OFDM signal reads in complex baseband notation:

$$\begin{aligned} s(t) &= s_{\rm p}(t) + s_{\rm d}(t) \\ &= \sum_{i \in \mathbf{I}_{\rm p}} s_i(t) + \sum_{i \in \mathbf{I}_{\rm d}} s_i(t) \end{aligned} \qquad (2)$$

with $s_i(t) = a_i e^{\jmath 2\pi n(i) \Delta f (t - k(i) T_{\rm p})} \mathbb{1}(\frac{t}{T_{\rm p}} - k(i) \in [-\frac{1}{2}, \frac{1}{2}])$. Here, a_i is the ith transmit symbol, $\jmath = \sqrt{-1}$, and $\mathbb{1}(\cdot)$ denotes the indicator function.

Assuming transmission across a multipath propagation channel, the received signal reads

$$Y(t) = \sum_{l=0}^{L-1} \alpha_l s(t, \boldsymbol{\theta}_l) + N(t) \qquad (3)$$

with $s(t, \boldsymbol{\theta}_l) = s(t - \tau) e^{\jmath 2\pi \nu_l t}$ where $s(t - \tau) = s_{\rm p}(t - \tau_l) + s_{\rm d}(t - \tau_l)$. The lth multipath component is characterized by its complex weight α_l, delay τ_l, and Doppler shift ν_l. We concatenate the later two parameters in the vector $\boldsymbol{\theta}_l = [\tau_l, \nu_l]^T$. The noise contribution $N(t)$ is assumed to be a circular white complex Gaussian process with autocorrelation

$$\mathrm{E}[N(t) N^*(t + \tau)] = N_0 \delta(\tau), \qquad (4)$$

where $\mathrm{E}[\cdot]$ denotes expectation, $(\cdot)^*$ stands for complex conjugation, N_0 is a positive constant, and $\delta(\cdot)$ is the Dirac delta function.

III. MAXIMUM-LIKELIHOOD ESTIMATION OF DELAY AND DOPPLER SHIFT

In this section, we first derive the joint maximum likelihood estimator of the delay and Doppler shift in an OFDM scenario with pilot-only transmission across a single-path propagation channel. Then, we define the pilot ambiguity function and derive the CRBs for the estimation of the delay and Doppler shift. Finally, we propose a constrained optimization problem for pilot signal design.

We assume a single-path propagation channel ($L = 1$) with complex gain α_0, delay τ_0 and Doppler shift ν_0[1]. Furthermore, the OFDM frame duration is short enough so that α_0, τ_0 and ν_0 are constant during one OFDM frame. Under these assumptions, the channel time-frequency response is flat in frequency, but varies from one OFDM symbol to another due to the Doppler shift. We define the signal to noise ratio (SNR) $\gamma = \frac{E_{\rm p}}{N_0}$ with $E_{\rm p} = \int |s_{\rm p}(t)|^2 {\rm d}t$.

We further assume that the receiver estimates the unknown parameter vector $\boldsymbol{\psi}_0 = [\boldsymbol{\theta}_0, \alpha_0]^T$ based only on the observation of the pilot signal, i.e. we set $s_{\rm d}(t) = 0$, and thus $s(t) = s_{\rm p}(t)$ and $s(t; \boldsymbol{\theta}_0) = s_{\rm p}(t; \boldsymbol{\theta}_0)$. From (3) and with the above assumptions, the log-likelihood function of $\boldsymbol{\psi} = [\boldsymbol{\theta}, \alpha]^T$ reads [9]

$$\tilde{\Lambda}(\boldsymbol{\psi}; Y(t)) = \frac{2}{N_0} \mathcal{R}\left\{\alpha^* \Lambda(\boldsymbol{\theta}; Y(t))\right\} - \frac{|\alpha|^2}{N_0} \int |s_{\rm p}(t; \boldsymbol{\theta})|^2 {\rm d}t. \qquad (5)$$

In this expression, $\mathcal{R}\{\cdot\}$ and $|\cdot|$ denote respectively the real part and the absolute value of the argument and $\Lambda(\boldsymbol{\theta}; Y(t)) = \int s_{\rm p}^*(t; \boldsymbol{\theta}) Y(t) {\rm d}t$. Note that the term $\int |s_{\rm p}(t; \boldsymbol{\theta})|^2 {\rm d}t = E_{\rm p}$ that arises in the log-likelihood function does not depend on $\boldsymbol{\theta}$. Given the pilot signal observation $Y(t) = y(t)$, the joint maximum likelihood (ML) estimator of the delay, Doppler and complex gain is

$$\hat{\boldsymbol{\psi}}_0 = \arg\max_{\boldsymbol{\psi}} \tilde{\Lambda}(\boldsymbol{\psi}; y(t)). \qquad (6)$$

The estimation problem in (6) is separable:

$$\hat{\boldsymbol{\theta}}_0 = \arg\max_{\boldsymbol{\theta}} |\Lambda(\boldsymbol{\theta}; y(t))|^2 \qquad (7)$$

$$\hat{\alpha} = \frac{\Lambda(\hat{\boldsymbol{\theta}}_0; y(t))}{E_{\rm p}}. \qquad (8)$$

[1]We will return to the multipath scenario in Section V.

Therefore, to estimate the delay and Doppler shift, we need to compute $\Lambda(\boldsymbol{\theta}; y(t))$. In practice, this computation can be implemented via a correlator which correlates the observed signal $y(t)$ with the delayed and Doppler shifted replicas of the pilot signal.

A. Ambiguity Function of Pilot Signals

We can rewrite the objective function in (7) as

$$\left| \underbrace{\int s_{\mathrm{p}}^{*}(t;\boldsymbol{\theta}) s_{\mathrm{p}}(t;\boldsymbol{\theta}_0)\mathrm{d}t}_{\chi(\boldsymbol{\theta},\boldsymbol{\theta}_0)} + \underbrace{\int s_{\mathrm{p}}^{*}(t;\boldsymbol{\theta}) N(t)\mathrm{d}t}_{W(\boldsymbol{\theta})} \right|^2. \quad (9)$$

The term $\chi(\boldsymbol{\theta}, \boldsymbol{\theta}_0)$ is the so-called ambiguity function of $s_{\mathrm{p}}(t)$ [10] and $W(\boldsymbol{\theta})$ is a zero mean colored Gaussian process.

The ambiguity function of the pilot signal limits the accuracy of the estimation of $\boldsymbol{\theta}_0$. To minimize the estimation error, $s_{\mathrm{p}}(t)$ shall be designed such that its ambiguity function exhibits a narrow main-lobe centered at $\boldsymbol{\theta}_0$ and low side-lobes [10]. However, due to the volume invariance property ($\iint |\chi(\boldsymbol{\theta}, \boldsymbol{\theta}_0)|^2 \mathrm{d}\tau \mathrm{d}\nu = 1$), the design involves a trade-off between the width of the main-lobe and the magnitude of the side-lobes [5]. Thus if $s_{\mathrm{p}}(t)$ is selected such that its ambiguity function exhibits a narrow main-lobe, high side-lobes may appear and vice-versa.

B. Fisher Information and Cramér-Rao Bound

In the subsequent investigation, we consider the real vector $\tilde{\boldsymbol{\psi}} = [\boldsymbol{\theta}, \mathcal{R}(\alpha), \mathcal{I}(\alpha)]^T$ with $\mathcal{I}\{\cdot\}$ denote the imaginary part of the argument. The Fisher information matrix for $\tilde{\boldsymbol{\psi}}$ is defined as [5]

$$\mathbf{J}(\tilde{\boldsymbol{\psi}}) = \mathrm{E}_{\tilde{\boldsymbol{\psi}}} \left[\frac{\partial}{\partial \tilde{\boldsymbol{\psi}}} \tilde{\Lambda}(\boldsymbol{\psi}; Y(t)) \left(\frac{\partial}{\partial \tilde{\boldsymbol{\psi}}} \tilde{\Lambda}(\boldsymbol{\psi}; Y(t)) \right)^H \right], \quad (10)$$

with $(\cdot)^H$ denoting hermitian transposition. Using (3) and (5), we obtain after some algebraic manipulations

$$\mathbf{J}(\tilde{\boldsymbol{\psi}}) = \gamma \frac{8\pi^2}{E_{\mathrm{p}}} \mathcal{R}\left\{ \mathbf{G}^{\mathbf{H}} \mathbf{M}(\tilde{\boldsymbol{\psi}}) \mathbf{G} \right\} \quad (11)$$

where

$$\mathbf{G} = \mathrm{diag}\{\mathbf{N}, \mathbf{1}, \mathbf{1}, \mathbf{1}\}$$

$$\mathbf{M}(\tilde{\boldsymbol{\psi}}) = \int \begin{bmatrix} |\alpha|^2 \Delta f^2 & -|\alpha|^2 t \Delta f & -\jmath\alpha \frac{\Delta f}{2\pi} & -\alpha \frac{\Delta f}{2\pi} \\ |\alpha|^2 t \Delta f & |\alpha|^2 t^2 & \jmath\alpha t & \alpha t \\ \jmath\alpha \frac{\Delta f}{2\pi} & -\jmath\alpha t & 1 & 0 \\ \alpha \frac{\Delta f}{2\pi} & -\alpha t & 0 & 1 \end{bmatrix} \otimes \mathbf{C}(\boldsymbol{\theta}, \boldsymbol{\theta}', t) \mathrm{d}t$$

with diag$\{\}$ stands for a block diagonal matrix with the column vector on its diagonal, $\otimes$ denoting the Kronecker product, $\mathbf{1}$ being a column vector of all ones, $\mathbf{N} = [n(1), n(2), \ldots, n(NK)]^T$, and $\mathbf{C}(\boldsymbol{\theta}, \boldsymbol{\theta}', t)$ denoting the $NK \times NK$ matrix with (i,j)th entry $s_i(t, \boldsymbol{\theta}) \mathbb{1}(i \in \mathbf{I}_{\mathrm{p}}) s_j^*(t, \boldsymbol{\theta}') \mathbb{1}(j \in \mathbf{I}_{\mathrm{p}})$.

The mth diagonal element of the inverted Fisher information matrix is the CRB on the variance of the estimation error of an unbiased estimator of $[\boldsymbol{\psi}_0]_m$. In particular,

$$\mathrm{CRB}_\tau = [\mathbf{J}^{-1}(\boldsymbol{\psi}_0)]_{1,1} \text{ and } \mathrm{CRB}_\nu = [\mathbf{J}^{-1}(\boldsymbol{\psi}_0)]_{2,2}. \quad (12)$$

The CRB is "local bound" in the sense that it depends essentially on the curvature of the main-lobe of the ambiguity function [5, Ch.10]. The narrower the main-lobe, the lower the CRB. As the SNR γ is a common factor that can be factored out from the Fisher information matrix (11), it is irrelevant when comparing the CRBs for various pilot signal selections. For such comparison, we can therefore consider the re-scaled versions $\gamma\mathrm{CRB}_\tau$ and $\gamma\mathrm{CRB}_\nu$.

C. Constrained Optimization Problem for Pilot Signal Design

It is well-known that the mean-squared error (MSE) of a nonlinear estimator such as (7) exhibits a so-called threshold effect [5]: If the SNR drops below a certain threshold value γ^{th}, there is an abrupt increase in the MSE of the estimator. We define γ^{th} for our particular application as follows:

Definition 1: The threshold value of a nonlinear estimator of (τ_0, ν_0) that asymptotically approaches the CRBs in (12) as the SNR increases is

$$\gamma^{th} = \max\{\gamma_{\hat{\tau}}^{th}, \gamma_{\hat{\nu}}^{th}\}$$

with

$$\gamma_{\hat{\tau}}^{th} = \min\{\gamma' : \mathrm{MSE}_{\hat{\tau}}(\gamma) \leq 2\mathrm{CRB}_\tau(\gamma) \text{ for all } \gamma > \gamma'\},$$
$$\gamma_{\hat{\nu}}^{th} = \min\{\gamma' : \mathrm{MSE}_{\hat{\nu}}(\gamma) \leq 2\mathrm{CRB}_\nu(\gamma) \text{ for all } \gamma > \gamma'\}.$$

The threshold effect is caused by outliers which occur if the estimate move from the main-lobe of the ambiguity function in (9) to one of its side-lobes due to noise. The probability that outliers occur at a particular SNR is closely connected to the magnitude of the highest side-lobe of the normalized ambiguity function [5] [11]. We define the normalized side-lobe level (NSL) as the magnitude of the highest side-lobe of the normalized ambiguity function. A high NSL leads to a high sensitivity of the estimator towards noise, therefore, leading to high γ^{th}. Determining γ^{th} requires time-consuming Monte Carlo simulations. As an alternative, we can numerically obtain the NSL with a much lower computational effort.

To keep γ^{th} low, the NSL needs to be minimized. At the same time, to minimize the estimation error when the SNR is larger than γ^{th}, the CRBs also need to be minimized. But there is a tradeoff between the NSL and the CRBs. To account for this tradeoff, we formulate the design of the pilot signal as a constrained optimization problem[2]:

[2]We could equally formulate another optimization problem which takes the NSL as constraint and minimizes the CRBs, i.e.

$$\begin{aligned} &\arg\min_{\mathbf{I}_{\mathrm{p}} \in \mathbf{I}} \mathrm{CRB}_\tau(\mathbf{I}_{\mathrm{p}}), \mathrm{CRB}_\nu(\mathbf{I}_{\mathrm{p}}) \\ &\text{subject to } |\mathbf{I}_{\mathrm{p}}| = N_{\mathrm{p}} \\ &\mathrm{NSL}(\mathbf{I}_{\mathrm{p}}) < \mathrm{NSL}(\mathbf{I}_0). \end{aligned}$$

In this case, however, one needs to simultaneously optimize two conflicting objectives (CRB_τ and CRB_ν). Indeed, reducing CRB_τ might increase CRB_ν and vice versa.

$$\begin{aligned} &\arg\min_{\mathbf{I}_\mathrm{p}\in\mathbf{I}} \mathrm{NSL}(\mathbf{I}_\mathrm{p}) \\ &\text{subject to } |\mathbf{I}_\mathrm{p}| = N_\mathrm{p} \\ &\mathrm{CRB}_\tau(\mathbf{I}_\mathrm{p}) < \mathrm{CRB}_\tau(\mathbf{I}_0), \\ &\mathrm{CRB}_\nu(\mathbf{I}_\mathrm{p}) < \mathrm{CRB}_\nu(\mathbf{I}_0), \end{aligned} \tag{13}$$

where $\mathbf{I}_0$ is a reference pilot signal with $|\mathbf{I}_0| = N_\mathrm{p}$.

The optimization procedure (13) differs from the optimization procedure formulated in [8] in three respects. First, whereas both procedures make use of the NSL as the first figure of merit, the former utilizes the CRBs as the second figure, while the latter utilizes the 3 dB bandwidth. Note that the CRBs can be easily computed via (12) and the NSL can be computed numerically. Second, while the latter procedure accounts for the tradeoff between the two figures of merit by specifying a weighted sum of them as the objective function to be optimized, the former deals with this tradeoff by means of a constrained optimization. Third, the procedure in [8] is constrained to the delay domain only, while (13) extends over the delay-Doppler domain.

IV. A GENETIC ALGORITHM FOR PILOT SIGNAL DESIGN

The global optimal solution to the above optimization problem may be in principle found by exhaustive search. However, this search is unfeasibly complex since the number of possible patterns is $\binom{NK}{N_\mathrm{p}}$, which is large even for moderate values of NK and N_p. A feasible alternative is to use a genetic algorithm. Genetic algorithms are easy to implement, have fast convergence and are able to avoid local extrema [12]. Although the obtained solutions are suboptimal, genetic algorithms are well-suited for combinatorial optimization problems. We refer the interested reader to [12] for the basics and the applications of such algorithms in signal processing.

We propose the genetic algorithm described below (Algorithm 1) to solve the constraint optimization problem (13). In this context, we define the "chromosomes" to be the pilot patterns. The algorithm can be conveniently extended to jointly design the pilot pattern and the pilot signature by additionally including the complex amplitudes in each chromosome.

V. NUMERICAL PERFORMANCE EVALUATION

In this section, we utilize the proposed Algorithm 1 to design pilot signals for delay-Doppler estimation and then compare their performance to state-of-the-art pilot signals via Monte Carlo simulations of the MSE for the joint delay-Doppler shift estimator in (7). For these investigations, we use the settings summarized in Table I. The considered OFDM frame corresponds to 24 resource blocks according to the LTE specifications.

In Fig. 2, we consider four pilot signals (a)-(d): Pattern (a) is the equispaced and equipowered pilot signal; Pattern (b) is the "perfect periodic" Costas array; Pattern (c) is the pilot pattern designed using Algorithm 1; and Pattern (d) is obtained using Algorithm 1 modified to design pilot pattern and signature jointly. Fig. 2 reports patterns (a)-(d), along with their associated magnitude of the ambiguity functions, NSLs, and CRBs. From the results in Fig. 2, we make two observations: Firstly, we observe that the pilot signal designed with Algorithm 1, i.e. (c) and (d), leads to much lower fitness parameters (NSL and CRBs) than that are obtained for (a) and (b). Thus, as expected, Algorithm 1 is able to improve the design of pilot signals in terms of their fitness parameters as expected. We remark that the noticeably high NSL of the ambiguity function associated with the "perfect periodic" Costas array (b) is induced jointly by the high side-lobes near the main-lobe of the ambiguity function of the Costas array and the repetition of this array with the selected spacing in the frequency domain. Secondly, we observe only small differences between the NSLs and the CRBs for pilot signals (c) and (d). This observation indicates that the impact of the pilot pattern is predominant on the estimator performance compared to the impact of the pilot signature.

We now evaluate the reduction of MSE that can be obtained for the pilot signals designed with Algorithm 1 by means of Monte Carlo simulations using the joint delay-Doppler shift estimator (7). We demonstrate that although Algorithm 1 is proposed under simplified conditions, the designed pilot signals are also appropriate under more re-

Algorithm 1: Genetic algorithm for the design of pilot pattern for joint delay-Doppler estimation.

$\leftarrow$: assignment operation.

URWR: uniformly at random without replacement.

Initialization: Set N_ind, N_elite(even number), N_m and randomly generate the initial population $\mathbf{I}(0) = \{\mathbf{I}_{p_1}, \ldots, \mathbf{I}_{p_{N_\mathrm{ind}}}\}$ with $|\mathbf{I}_{\mathrm{p_i}}| = N_p$;

for $g = 0, 1, \ldots, MaxGen$ **do**

Elite selection: Form $\mathbf{I}_\mathrm{elite}(g) \subset \mathbf{I}(g)$ consisting of the N_elite pilot patterns with the lowest fitness

$$F(\mathbf{I}_{\mathrm{p_i}}) = \begin{cases} \text{NSL} & \mathrm{CRB}_\tau(\mathbf{I}_{\mathrm{p_i}}) < \mathrm{CRB}_\tau(\mathbf{I}_0) \ \& \\ & \mathrm{CRB}_\nu(\mathbf{I}_{\mathrm{p_i}}) < \mathrm{CRB}_\nu(\mathbf{I}_0) \quad ; \\ 1 & \text{otherwise.} \end{cases}$$

$\mathbf{I}(g+1) \leftarrow \mathbf{I}_\mathrm{elite}(g)$;

for $j = 1, \ldots, \frac{N_\mathrm{elite}}{2}$ **do**

Pick two elements $\mathbf{I}^{'}, \mathbf{I}^{''} \in \mathbf{I}_\mathrm{elite}(g)$ URWR ;

Generate offspring $\mathbf{I}_\mathrm{off} \subset \mathbf{I}^{'} \cup \mathbf{I}^{''}$ by picking N_p elements from $\mathbf{I}^{'} \cup \mathbf{I}^{''}$ URWR ;

Mutation: Pick N_m elements from $\mathbf{I}_\mathrm{off}$ URWR and substitute them by N_m elements picked from $\mathbf{I}^\mathrm{c}_\mathrm{off} = \mathbf{I} \setminus \mathbf{I}_\mathrm{off}$ URWR to generate $\mathbf{I}_\mathrm{m}$;

$\mathbf{I}_\mathrm{elite}(g) \leftarrow \mathbf{I}_\mathrm{elite}(g) \setminus \{\mathbf{I}^{'}, \mathbf{I}^{''}\}$;

Update population: $\mathbf{I}(g+1) \leftarrow \mathbf{I}(g+1) \cup \mathbf{I}_\mathrm{m}$;

end

end

TABLE I

SIMULATION SETTINGS

OFDM system:
N = 288, K = 7, N_{p} = 96
$T_{\mathrm{p}} = T + T_{\mathrm{cp}} = 66.7 + 6.67 = 73.4\,\mu\mathrm{s}$
Genetic algorithm:
$N_{\mathrm{ind}} = 100$, $N_{\mathrm{elite}} = 40$, $N_{\mathrm{m}} = 1$, $MaxGen = 80$
$\mathbf{I}_0$ = "Perfect periodic" Costas array
Estimation range $\tau \in [-\frac{T_{\mathrm{p}}}{2}, \frac{T_{\mathrm{p}}}{2}]$, $\nu \in [-\frac{\Delta f}{2}, \frac{\Delta f}{2}]$
Pilots are equipowered with zero phase unless otherwise specified.

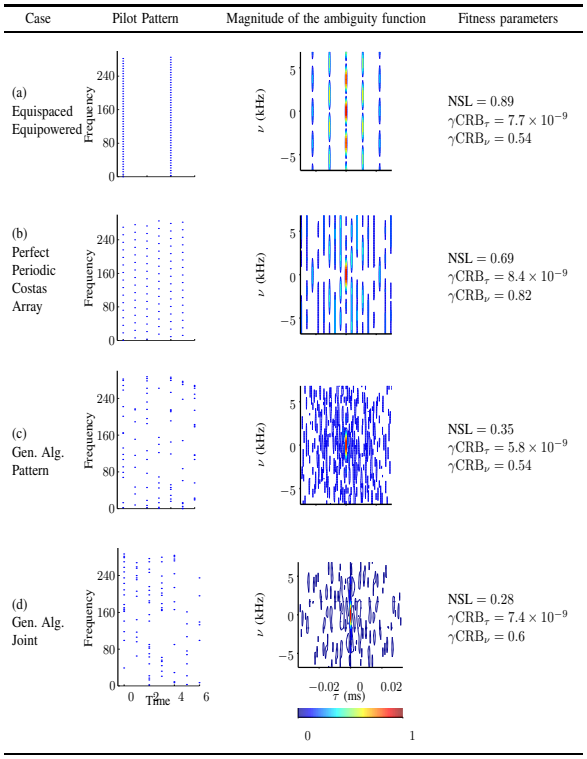

Fig. 2. The considered pilot signals. The pilot pattern and signature of the pilot signal in panel (d) are jointly optimized: the amplitudes and phases of all pilots are drawn independently according to a uniform distribution on $[0, 1]$ and $[0, 2\pi]$ respectively during the initialization of Algorithm 1. At each mutation stage of the algorithm, the signature of the N_{m} selected pilots is drawn similarly. After each random drawing, the pilot signature is scaled such that its energy equals 1.

alistic conditions. We consider three scenarios of increasing realism: Scenario 1 is the single-path propagation with pilot-only transmission, i.e. the scenario for which estimator (7) coincides with the maximum likelihood estimator of the delay and Doppler shift. Scenario 2 is the same as Scenario 1, but includes data transmission. Scenario 3 is with both data transmission and multipath propagation. In the first two scenarios, we assume without loss of generality that $\psi_0 = [0, 0, 1]^T$.

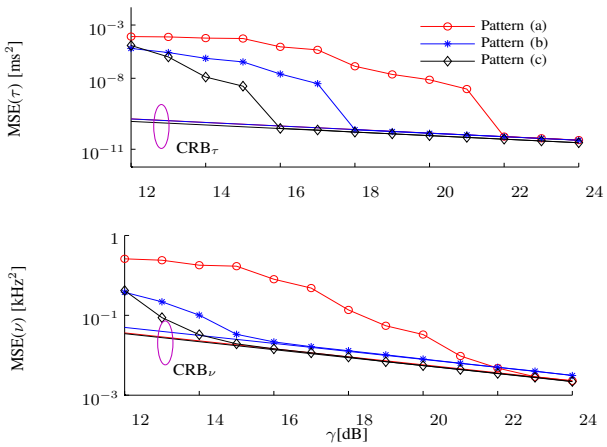

Fig. 3. Scenario 1: MSE performance of estimator (7) and CRBs versus SNR when using pilot patterns (a), (b), and (c) in Fig. 2. The corresponding threshold values (γ^{th}) are 23 dB, 18 dB and 16 dB, respectively. Each point is obtained from 10000 Monte Carlo trials.

A. Scenario 1: Single-Path Propagation, Without Data Transmission

Fig. 3 reports the MSE of estimator (7) computed from Monte Carlo simulations, using pilot signals (a)-(c) in Fig. 2. It appears that pilot signal (c) designed with Algorithm 1 leads to a threshold gain of 7 dB and 2 dB compared to pilot signals (a) and (b) respectively, as a result of the significant reduction of the NSL.

B. Scenario 2: Single-Path Propagation, With Data Transmission

So far the effect of data signals on the estimation performance of the estimator (7) has been neglected in the literature, see e.g. [2] [4] [6] [8]. In this subsection, we compare the effect of data signals on patterns (b) and (c).

During the data transmission phase, (3) reads $Y(t) = \alpha_0(s_{\mathrm{p}}(t;\boldsymbol{\theta}_0)+s_{\mathrm{d}}(t;\boldsymbol{\theta}_0))+N(t)$. The objective function in (7) is given by

$$\begin{aligned} Z(\boldsymbol{\theta}; Y(t)) &= \left| \int s_{\mathrm{p}}^*(t;\boldsymbol{\theta}) Y(t) \mathrm{d}t \right|^2 \\ &= \Big| \alpha_0 \chi(\boldsymbol{\theta}, \boldsymbol{\theta}_0) + \underbrace{\alpha_0 \int s_{\mathrm{p}}^*(t;\boldsymbol{\theta}) s_{\mathrm{d}}(t;\boldsymbol{\theta}_0) \mathrm{d}t}_{\text{Interference}} \\ &\quad + W(\boldsymbol{\theta}) \Big|^2. \end{aligned} \tag{14}$$

Fig. 4 reports the MSE of estimator (7) when using pilot signals (b) and (c). A comparison with the MSE results reported Fig. 3 shows that the interference caused by data transmission only affects the threshold value, which is shifted to the right by approximately 1 dB. In the high SNR regime, the data interference has no significant effect on the estimator performance.

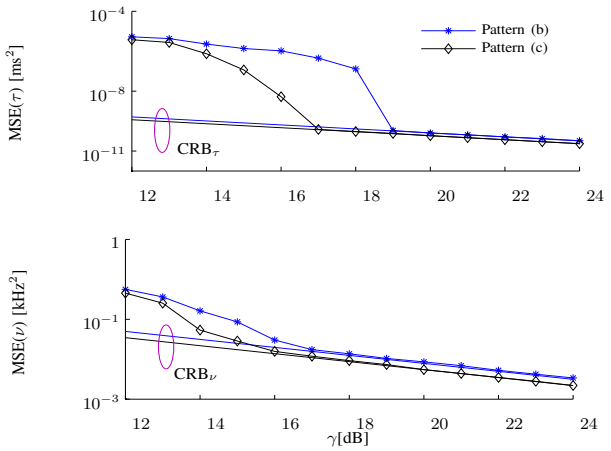

Fig. 4. Scenario 2: MSE performance of estimator (7) and CRBs versus SNR when using pilot patterns (b) and (c) in Fig. 2. Each point is obtained from 10000 Monte Carlo trials.

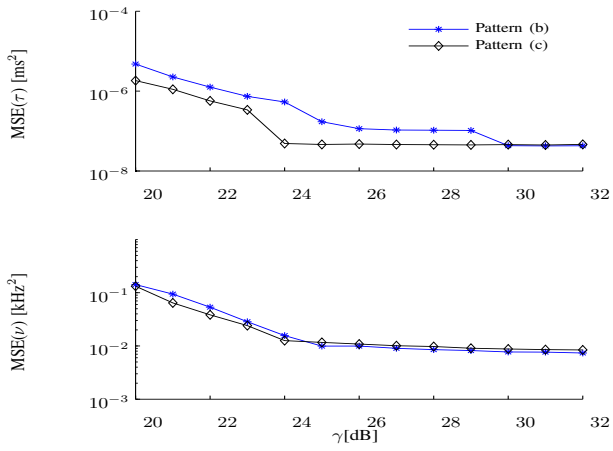

Fig. 5. Scenario 3: MSE performance of estimator (7) versus SNR when using pilot patterns (b) and (c) in Fig. 2. Each point is obtained from 10000 Monte Carlo trials.

C. Scenario 3: Multipath Propagation, With Data Transmission

In the third and most realistic scenario, we consider both data transmission and multipath propagation. In this scenario, the objective function (7) reads

$$Z(\boldsymbol{\theta};Y(t)) \;=\; \Big|\sum_{l=0}^{L-1}\alpha_l\chi(\boldsymbol{\theta},\boldsymbol{\theta}_l) + \underbrace{\sum_{l=0}^{L-1}\alpha_l\int s_{\mathrm{p}}^*(t;\boldsymbol{\theta})s_{\mathrm{d}}(t;\boldsymbol{\theta}_l)\mathrm{d}t + W(\boldsymbol{\theta})}_{\text{Interference}}\Big|^2 \quad (15)$$

First we consider the case where the main-lobe and the side-lobes of the ambiguity function of the pilot signal devised with Algorithm 1 are respectively sufficiently narrow and low enough, so that the L multipath components can be resolved in the delay-Doppler domain. This implies that, if one discards the effect of noise and data interference in (15), $Z(\boldsymbol{\theta};Y(t))$ exhibits L well-separated dominant peaks, each peak being contributed by one multipath component. Each peak uniquely corresponds to the main-lobe of one of the weighted ambiguity function in the first summand in (15). In this case, the joint ML estimator of the L pairs $\{(\tau_l,\nu_l)\}_{l=1}^{L}$ is accurately approximated by L independent ML estimators, one for each pair. The outputs of these L estimators are the L delay-Doppler arguments corresponding to the L largest maxima of $Z(\boldsymbol{\theta};Y(t))$. The same approximation holds true in the presence of data interference and of noise at high SNR and even at medium SNR since the NSL is low. Thus, in a scenario with well-separable multipath components, a pilot signal designed using Algorithm 1 still essentially keeps its optimality properties in medium and high SNR regime.

A necessary condition for multipath components to be separable is that the bandwidth of the OFDM system is large enough. Due to practical constraints on the available bandwidth of the OFDM system and the number of pilots, not all path components may be resolved in $Z(\boldsymbol{\theta};y(t))$ in (15). We consider such a case in the following and show that the pilot pattern designed using Algorithm 1 is still a good choice. We use (7) to obtain the delay and Doppler shift estimates and compute the MSE of the delay and Doppler shift by using the first path component as the reference. As indicated in the introduction, this estimate can be used—in combination with other such estimates computed from other transmission links—for localization in a TOA or TDOA based positioning method, or also for synchronization [13]. However, due to the unresolvable path components with higher delay than the first component, the estimator is expected to be biased.

The "Extended Vehicular A" channel model specified in the 3GPP LTE standard [14] is used to generate a new channel impulse response for each simulation trial. The values of the delay, Doppler shift and weight magnitude of the $L = 9$ multipath components are kept fixed while generating the channel responses. The phases of the path weights are drawn independently from a uniform distribution on $[0, 2\pi)$ for each trial.

A comparison of the MSE curves depicted in Fig. 5 with those reported in Fig. 4 shows that a much higher error floor appears at high SNR due to bias caused by unresolved multipath components. In addition, the multipath channel leads to a significantly shifts of the thresholds. Specifically, for the pilot signal designed with Algorithm 1, a pronounced threshold appears at 25 dB while for the "perfect periodic" Costas array, it appears at 30 dB. This observation indicates that even though pilot pattern (c) is optimized for the idealized scenario ignoring multipath propagation and data transmission, it still leads to better performance than obtained by using the "perfect periodic" Costas array.

VI. CONCLUSION

The conventional equispaced and equipowered pilot signals, as used in LTE, is suboptimal for joint delay and Doppler estimation. It has an ambiguity function with a high normalized side-lobe level (NSL), which causes the

correlator-based estimator (7) to exhibit a high threshold value. The proposed genetic algorithm generates pilot signals that minimize the NSL, while maintaining the CRBs for the delay and Doppler shift estimation below a target value. Compared to the "perfect periodic" Costas arrays, these pilot signals produce much lower NSL and CRBs. The results clearly exemplify that the possible reduction in MSE can be achieved with the same number of pilots. An additional finding is that the pilot pattern affects more significantly the NSL and the CRBs than the pilot signature does. Our genetic algorithm can generate close-to-optimal pilot signals regardless of the OFDM frame size and the number of pilots. This computation can be done offline. We also show that the pilot signals computed with the genetic algorithm remain a good choice in single-path and multipath propagation conditions during the data transmission phase when a correlator is employed for delay and Doppler shift estimation.

Among the interesting open research avenues, we would like to mention the extension of the constrained optimization problem to account for transmission across multipath channels, especially when more sophisticated channel estimators are used. The performance of these estimators could then be assessed by means of performance criteria traditionally employed in communications, such as channel estimation error and bit-error-rate.

ACKNOWLEDGMENT

This work has been funded by the project ICT-248894 Wireless Hybrid Enhanced Mobile Radio Estimators–Phase 2 (WHERE2).

REFERENCES

[1] L. Tong, B. Sadler, and M. Dong, "Pilot-assisted wireless transmissions: general model, design criteria, and signal processing," *IEEE Signal Process. Mag.*, vol. 21, no. 6, pp. 12–25, Nov. 2004.

[2] A. Sayed, A. Tarighat, and N. Khajehnouri, "Network-based wireless location," *IEEE Signal Process. Mag.*, vol. 22, no. 4, pp. 24–40, 2005.

[3] P. Chestnut, "Emitter location accuracy using TDOA and differential doppler," *IEEE Trans. Aerosp. Electron. Syst.*, vol. AES-18, no. 2, pp. 214–218, Mar. 1982.

[4] A. Dammann, C. Mensing, and S. Sand, "On the benefit of location and channel state information for synchronization in 3GPP-LTE," in *European Wireless Conf.*, 2010, pp. 711–717.

[5] H. L. Van Trees, *Detection, Estimation, and Modulation Theory - Part III*. John Wiley & Sons, 2001.

[6] J.-C. Guey, "Synchronization signal design for OFDM based on time-frequency hopping patterns," in *IEEE International Conf. on Commun.*, 2007, pp. 4329–4334.

[7] J. Costas, "A study of a class of detection waveforms having nearly ideal range-Doppler ambiguity properties," *Proc. IEEE*, vol. 72, no. 8, pp. 996–1009, Aug. 1984.

[8] O. Ureten, S. Tascioglu, N. Serinken, and M. Yilmaz, "Search for OFDM synchronization waveforms with good aperiodic autocorrelations," in *Canadian Conf. on Elect. and Compt. Eng.*, vol. 1, May 2004, pp. 13–18.

[9] H. Poor, *An Introduction to Signal Detection and Estimation*. Springer-Verlag, 1994.

[10] P. Woodward, *Probability and Information Theory, with Applications to Radar*. Pergamon Press, 1953.

[11] F. Athley, "Threshold region performance of maximum likelihood direction of arrival estimators," *IEEE Trans. Signal Process.*, vol. 53, no. 4, pp. 1359–1373, Apr. 2005.

[12] K. Tang, K. Man, S. Kwong, and Q. He, "Genetic algorithms and their applications," *IEEE Signal Process. Mag.*, vol. 13, no. 6, Nov. 1996.

[13] C. Mensing, "Location Determination in OFDM Based Mobile Radio Systems," Ph.D. dissertation, Technische Universität München, 2013.

[14] 3GPP, "Base station (BS) radio transmission and reception," vol. 3GPP TS 36.104, V8.12.0 (2011-06) Technical Specification, 2011.